PROCEEDINGS OF THE ROYAL SOCIETY A

Proc. R. Soc. A (2006) **462**, 1021–1041
doi:10.1098/rspa.2005.1604
Published online 17 January 2006

An underwater shock simulator

By V. S. Deshpande, A. Heaver and N. A. Fleck*

Department of Engineering, University of Cambridge, Trumpington Street, Cambridge CB2 1PZ, UK

An underwater shock simulator has been developed for the underwater shock loading of materials and test structures within the laboratory. The tube is struck at one end by a steel projectile, with the test structure placed at the opposite end of the tube. Realistic exponentially decaying pressure pulses are generated in the water with peak pressures in the range 15–70 MPa and decay times ranging from 0.1 to 1.5 ms. The peak pressure and the pulse duration are independently adjusted by varying the projectile velocity and mass, respectively. The underwater shock simulator is used to investigate the one-dimensional fluid–structure interaction of sandwich plates with steel face sheets and an aluminium foam core. The degree of core compression is measured as a function of both the underwater shock impulse and the Taylor fluid–structure interaction parameter. Fully coupled finite element simulations agree well with the measurements while decoupling the fluid–structure interaction phase from the core compression phase within the finite element analysis leads to an under-prediction of the degree of core compression.

Keywords: fluid–structure interaction; sandwich structures; dynamic plasticity

1. Introduction

In his pioneering paper, Taylor (1941) computed the momentum transmitted to a free-standing plate due to the impingement of a one-dimensional underwater shock wave. The fraction of the incoming shock momentum that is transmitted to the plate depends upon the impedance mismatch between the fluid and plate. For example, a light plate leads to early cavitation of the water and to a small fraction of the shock impulse transmitted into the structure. The subject of this paper is the development of an apparatus to investigate the underwater shock response of structures in a laboratory setting.

Recently, sandwich construction has been suggested as a means to enhance the fluid–structure interaction (FSI) effect and thereby increase the shock resistance of underwater structures. The reduced mass of the sandwich front face sheet leads to a reduction in the impulse transmitted to the structure compared to that transmitted into a monolithic structure of equal total mass. A number of studies have employed the Taylor (1941) free-standing plate model to investigate the underwater shock response of sandwich structures. For example, Fleck & Deshpande (2004) and Xue & Hutchinson (2004) estimated the shock resistance of clamped sandwich beams by decoupling the FSI phase from the subsequent

* Author for correspondence (naf1@eng.cam.ac.uk).

Received 6 August 2005
Accepted 31 October 2005

structural response. This approximation assumes that the time period for FSI phase is much shorter than the structural response time for plastic bending and stretching of the beam. However, in sandwich structures, core compression can occur on a similar timescale to the FSI phase. The significance of the overlap of timescales has been determined recently, as follows.

Rabczuk *et al.* (2004) investigated the response of sandwich beams subjected to underwater shocks by performing fully-coupled FSI simulations. Their finite element (FE) calculations suggest that the benefits of sandwich construction for shock mitigation applications might be overestimated by the analysis of Fleck & Deshpande (2004) and Xue & Hutchinson (2004). The questionable assumption in these earlier analyses is the decoupling of the FSI phase from the core compression phase. Hutchinson & Xue (2005) and Deshpande & Fleck (2005) have proposed modifications to the one-dimensional Taylor (1941) model to account for the presence of the core and rear face sheet in the FSI calculations. These studies confirm that the level of impulse transmitted into a sandwich plate is somewhat under-estimated by employing the Taylor free-standing plate analysis. The discrepancy in the transmitted impulse is typically of order 30%.

Only limited data exist on the shock response of structures. Florence (1966) and Menkes & Opat (1973) performed impulsive loading experiments on clamped plates and beams by placing sheet explosives in direct contact with the plates. More recently, Nurick & Martin (1989*a*) and Olsona *et al.* (1993) have measured and predicted the deformation and failure of impulsively loaded thin plates. They used a ballistic pendulum to measure the impulse imparted to the plate due to denotation of the explosive. Underwater blast loading experiments are typically conducted by detonating explosives at some distance from the test structures. Following the pioneering work of Taylor (1941), numerous researchers have investigated the deformation of plates subjected to an underwater blast; see Nurick & Martin (1989*a*,*b*) for a review of the relevant literature. Experimental studies into the tensile and shear failure mechanisms of rectangular steel plates have recently been conducted by Ramajeyathilagam *et al.* (2000) and Ramajeyathilagam & Vendhan (2004). All of these experimental techniques involve explosives and are difficult to perform in non-military laboratory settings.

An alternate method for simulating air blast loading is based upon the principle of the shock tube as used extensively in supersonic gas dynamics. The rupture of a diaphragm separating the low and high-pressure gas chambers in the shock tube results in a shock wave travelling down the low-pressure chamber and impinging upon the test structure at the remote end of the chamber. Gerard (1956) and Stoffel *et al.* (2001) have used this principle to investigate the air blast response of clamped plates. The aim of the present study is to introduce a safe, simple and robust underwater shock simulator for laboratory use and then employ the apparatus to investigate the one-dimensional underwater shock response of sandwich plates.

2. Basic principle of the laboratory underwater shock simulator

The underwater detonation of a high explosive charge converts the solid explosive material into gaseous reaction products (on a time scale of microseconds). The reaction products are at an enormous pressure (on the order of gigapascals), and this pressure is transmitted to the surrounding water by the propagation of a

spherical shock wave at approximately sonic speed. Consider the response of a representative fluid element at a radial distance r from the explosion. Upon arrival of the primary shock wave, the pressure rises to a peak value P_o almost instantaneously. Subsequently, the pressure decreases at a nearly exponential rate, with a time constant θ on the order of milliseconds, and is such that

$$p(t) = p_o \exp\left(\frac{-t}{\theta}\right), \tag{2.1}$$

where t is measured from the instant of arrival of the primary shock wave. The magnitude of the shock wave peak pressure and decay constant depend upon the mass and type of explosive material and upon the stand-off distance r. The damped oscillation of the gas bubble containing the explosive reaction products leads to secondary shocks. These secondary shock waves have much smaller peak pressures than the primary shock, and are usually much less damaging.

Experimental data (and physical models) support the use of simple power-law scaling relations between the mass m_e of explosive, the separation r between explosion and point of observation, and the resulting characteristics, p_o and θ of the primary shock. For example, for an underwater TNT explosion, the peak pressure (in megapascals) is taken from Table 2 of Swisdak (1978) as

$$p_o = 52.4\left(\frac{m_e^{1/3}}{r}\right)^{1.13} \text{MPa}, \tag{2.2}$$

where m_e is in kilograms, and r is in metres. The time constant θ (in milliseconds) is

$$\theta = 0.084 m_e^{1/3}\left(\frac{m_e^{1/3}}{r}\right)^{-0.23} \text{ms}. \tag{2.3}$$

These relations have been validated for the domain of m_e and r such that p_o lies in the range 3–140 MPa, see Swisdak (1978) for further details. Similar scaling relations have been obtained for other high explosives, and the coefficients in the above relations hold to reasonable accuracy for them also.

A shock simulator should simulate the underwater pressure pulse (2.1) in a laboratory setting without requiring detonation of an explosive charge. Moreover, we aim to control the peak pressure p_o and the decay time θ independently in order to conduct controlled experiments on the interaction of structures with underwater shocks.

The basic working principle of the laboratory underwater shock simulator is illustrated in figure 1. Consider the one-dimensional problem of a semi-infinite ($x \geq 0$) water column impacted at $x=0$ by a rigid striker of mass per unit area m travelling at an initial velocity v_o. With time t being measured from the instant of impact, let $p(t)$ be the pressure in the water at $x=0$. Employing an acoustic approximation, the particle velocity of the water at $x=0$ is given by

$$v = \frac{p}{c_w \rho_w}, \tag{2.4}$$

where c_w is the velocity of sound in water and ρ_w is the density of water. The striker is assumed to remain in contact with the water, and continuity at the interface dictates that the striker too has a velocity v at time t. Thus,

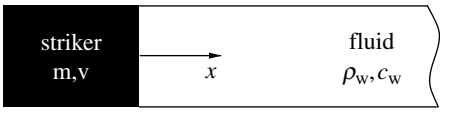

Figure 1. Diagram showing the basic principle of the underwater shock simulator with the coordinate system employed.

the equation of motion of the striker is

$$m\dot{v} = -p = -\rho_w c_w v, \tag{2.5}$$

where the over-dot denotes differentiation with respect to time. Employing the initial condition, $v = v_o$ at $t = 0$, the pressure $p(t)$ at $x = 0$ follows as

$$p = \rho_w c_w v_o \exp\left[-\frac{t}{m/(\rho_w c_w)}\right]. \tag{2.6}$$

This pressure wave travels along the fluid column at the speed c_w, with the pressure at any fixed position x given by

$$p(x,t) = \begin{cases} \rho_w c_w v_o \exp\left(-\dfrac{t - x/c_w}{m/(\rho_w c_w)}\right), & t \geq \dfrac{x}{c_w}, \\ 0, & \text{otherwise.} \end{cases} \tag{2.7}$$

Thus, the pressure versus time history is of the same form as that given in relation (2.1) for a spherical explosion. The peak pressure and decay times are given by

$$p_o = \rho_w c_w v_o, \tag{2.8a}$$

and

$$\theta = \frac{m}{\rho_w c_w}, \tag{2.8b}$$

respectively. Note that the peak pressure and the decay constant can be set independently by suitable adjustment of the striker velocity and mass.

3. Construction and validation of the shock simulator

We proceed to describe the experimental apparatus used to simulate an underwater shock wave by employing the principle described in §2.

(a) *Description of the experimental apparatus*

The experimental apparatus is sketched in figure 2*a*. A water column is located in a steel tube of length $L = 1.4$ m, internal diameter $D = 45$ mm and wall thickness $w = 7$ mm. The tube is capped at one end with a 6 mm thick aluminium piston while the test structure (described subsequently) is placed at the opposite end. The piston has an O-ring seal and contains a bleed valve to ensure that air is not trapped in the water column. Preliminary experiments reveal that trapped air in the water column attenuates the shock wave generated within the water column: the time required to attain the peak pressure is substantially increased and the peak pressure is reduced.

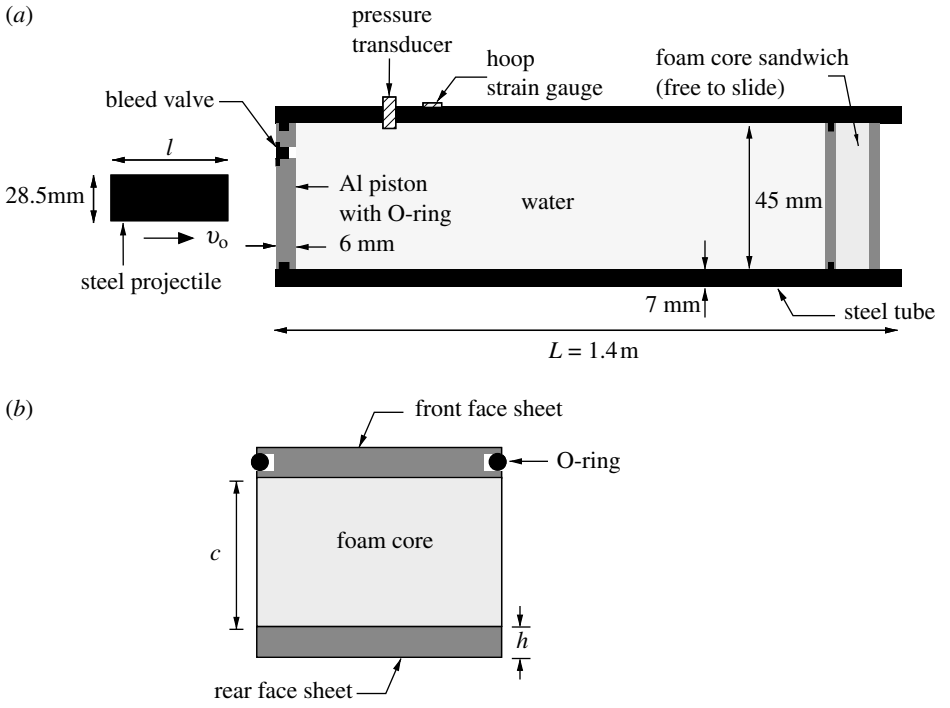

Figure 2. (*a*) Schematic of the water tube experimental set-up (not to scale) and (*b*) a sketch of the foam core sandwich test specimen.

Dynamic loading is achieved by firing a steel circular cylindrical projectile of diameter $d=28.5$ mm and mass in the range 0.2–2.5 kg at the Al piston of the water tube. The water tube is aligned such that the projectile impacts the piston centrally and normally. Oblique impact results in the generation of a non-planar shock wave. The projectiles are accelerated using a gas gun of barrel length 4.5 m and diameter 28.5 mm. No sabot is employed, and the bursting of copper shim diaphragms forms the breech mechanism of the gas gun. The projectile velocity ranges from 10 to 50 m s^{-1}, and is measured at the exit of the barrel using laser-velocity gates. The pressure transient in the water tube was measured using a high-frequency piezoelectric pressure sensor[1]. This pressure transducer, with an in-built charge amplifier, is specifically designed for shock tube and blast wave measurements. It has a dynamic measurement range of 0–69 MPa, a rise time of less than 1 μs and a resonant frequency exceeding 500 kHz. A hoop strain-gauge on the outer wall of the steel tube is used to confirm the accuracy of the pressure history. The hoop strain ϵ_{h} is related to the thin-walled cylindrical pressure by

$$p(t) = \frac{2Ew\epsilon_{\mathrm{h}}(t)}{D+w}, \tag{3.1}$$

where $E=210$ GPa is the Young's modulus of steel (the tube material). The elastic hoop strain history is monitored using a 120 Ω Techni Measure Ltd foil gauge of length 1 mm in a quarter Wheatstone bridge configuration, with a strain

[1] Model 102A03 of PCB Piezotronics Inc., 3425 Walden Avenue, Depew, NY 14043-2495, USA.

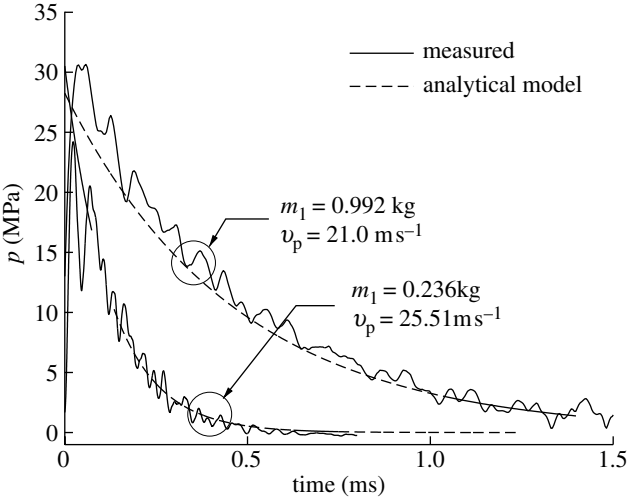

Figure 3. Comparison between the measured and predicted pressure versus time histories for two selected values of the projectile mass m_1. In both cases, the combined velocity of the piston and projectile $v_o \approx 20\ \mathrm{m\ s^{-1}}$.

bridge amplifier of cut-off frequency 500 kHz. The pressure transducer and hoop strain gauge are located approximately 100 mm from the impact end of the tube and a digital storage oscilloscope is used to record the output from these gauges.

The steel tube has a yield strength of 250 MPa, and so the apparatus described above can be used generate water pressures of up to 80 MPa. The maximum pulse duration θ is 1.5 ms, as longer pulses are corrupted by reflections from the structure.

(*b*) *Measurements of the pressure versus time histories*

We first conducted a series of experiments to measure the pressure versus time histories generated in the water column. The aim of this initial investigation is to validate the basic principle described in §2. Instead of employing a test structure in these experiments, an Al piston (similar to the one at the impact end) was fitted at the distal end of the tube to seal the water column. Unless otherwise stated, the pressure versus time histories reported below were measured using the piezoelectric pressure transducer.

Typical pressure versus time histories generated in the water shock tube are plotted in figures 3 and 4. The measurements in figure 3 show the effect of the projectile mass ($m_1 = 0.236$ and 0.992 kg) for a projectile impact velocity $v_p \approx 20\ \mathrm{m\ s^{-1}}$. In both experiments, the pressure rises sharply to an initial peak pressure $p_o \approx 28$ MPa followed by a decay to zero pressure over approximately 0.5 and 1.5 ms for the 0.236 and 0.992 kg projectiles, respectively. The effect of the impact velocity is illustrated in figure 4, where the measured pressure histories are plotted for the 0.236 kg projectile impacting at $v_p = 25.5\ \mathrm{m\ s^{-1}}$ and $39.3\ \mathrm{m\ s^{-1}}$. For both impact velocities, the peak pressure is attained in approximately 10 μs and the pulse duration is about 0.5 ms with the peak pressure higher for $v_p = 39.3\ \mathrm{m\ s^{-1}}$. These results are qualitatively consistent with the ideas presented in §2, i.e. the peak pressure and pulse duration are independently controlled by changing the striker velocity and mass, respectively.

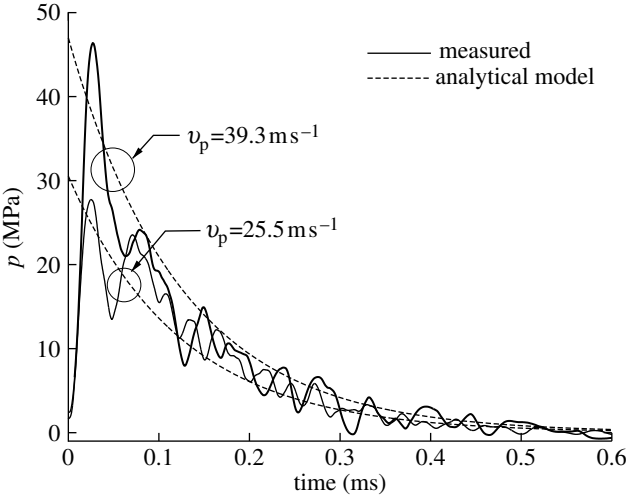

Figure 4. Comparison between the measured and predicted pressure versus time histories for two selected values of the projectile velocity v_p. In both cases, the projectile mass $m_1 = 0.236$ kg.

A comparison of the pressure history as measured by the pressure transducer and the hoop strain gauges is shown in figure 5 for the 0.236 kg projectile. Good agreement between the two sets of measurements is observed at $v_p = 34.6\ \mathrm{m\,s^{-1}}$ (figure 5*a*). However, significant 'ringing' is seen in the hoop strain measurements for $v_p = 17.5\ \mathrm{m\,s^{-1}}$ (figure 5*b*) resulting in poor agreement between the pressure measurements obtained from the strain gauge and the pressure transducer. We conclude that a hoop strain gauge is adequate for measuring the pressure histories for peak pressures $p_o \geq 40$ MPa, but only the pressure transducer has the required sensitivity for measuring lower pressures.

(*c*) *Comparison with predictions*

We now compare the measured pressure versus time histories with the predictions of §2. Recall that the one-dimensional model comprised a semi-infinite water column and a striker. In the experiments, a projectile of diameter $d = 28.5$ mm is fired at a stationary piston of diameter $D = 45$ mm; in-turn this piston loads the water column of diameter D. Assuming an inelastic collision between projectile and piston, the mass per unit area m and velocity v_o of the striker to be used in equation (2.8*a*,*b*) are given by

$$m = 4\frac{m_1 + m_2}{\pi D^2} \tag{3.2a}$$

and

$$v_o = \frac{m_1 v_p}{m_1 + m_2}, \tag{3.2b}$$

respectively, where m_1 and m_2 are the masses of the projectile and piston, respectively. The analytical predictions for the pressure versus time histories are included in figures 3 and 4 for these definitions for v_o and m. The model assumes

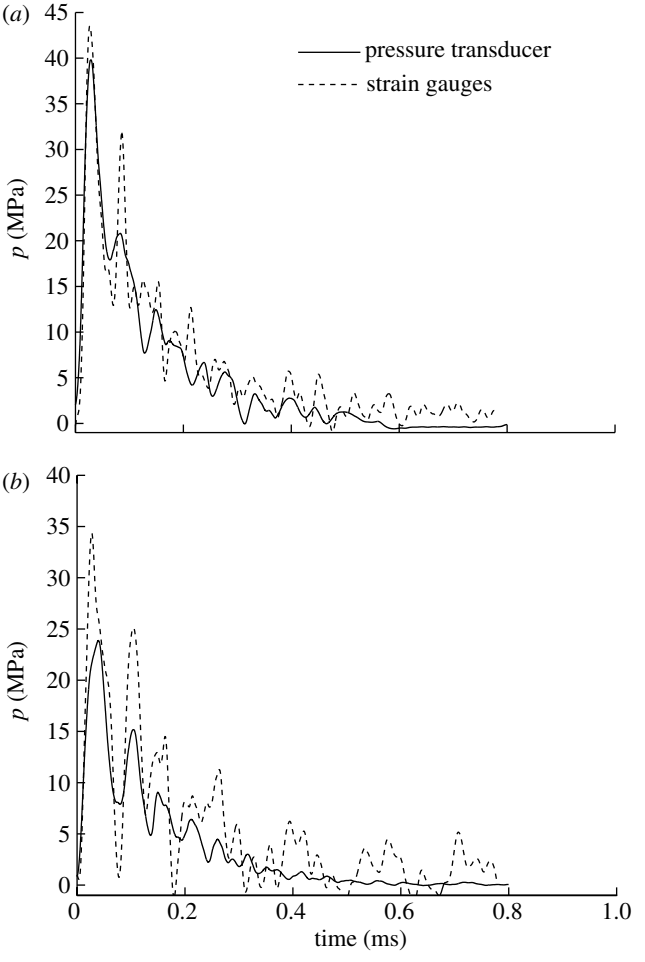

Figure 5. Comparison between the pressure versus time histories obtained from the pressure transducer and hoop strain gauges on the wall of the shock tube. The experiments were performed with $m_1 = 0.236$ kg and (*a*) $v_p = 34.6$ m s^{-1} and (*b*) $v_p = 17.5$ m s^{-1}.

the striker to be rigid giving an instantaneous rise to the peak pressure p_o while a finite rise time of about 10 μs is observed. Other than this small discrepancy, excellent agreement is noted between prediction and the measurement.

A series of experiments using five projectile masses and selected projectile velocities v_p in the range 10–50 m s^{-1} were performed to gauge the accuracy of the revised model. The dependence of peak pressure upon velocity v_o is summarized in figure 6 for the five projectile masses. The prediction (2.8*a*) is included in figure 6: excellent agreement between prediction and experiment is obtained. The peak pressure p_o increases linearly with velocity v_o and is almost independent of projectile mass. The measured decay time θ is estimated from a least-squares fit of the relation (2.1) to the measured data beyond peak pressure. These decay times are plotted in figure 7 as a function of the areal mass m defined by (3.2*a*). A set of data points at each value of m correspond to experiments at different striker velocities (figure 6). The analytical prediction (2.8*b*) of the variation of θ with m is

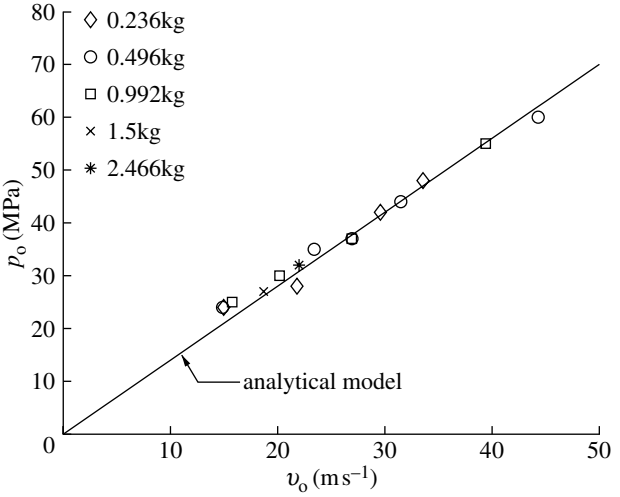

Figure 6. Comparison between the measured and predicted peak pressures p_o as a function of the resultant velocity v_o of the combined piston and projectile. Results are plotted for five projectile masses m_1.

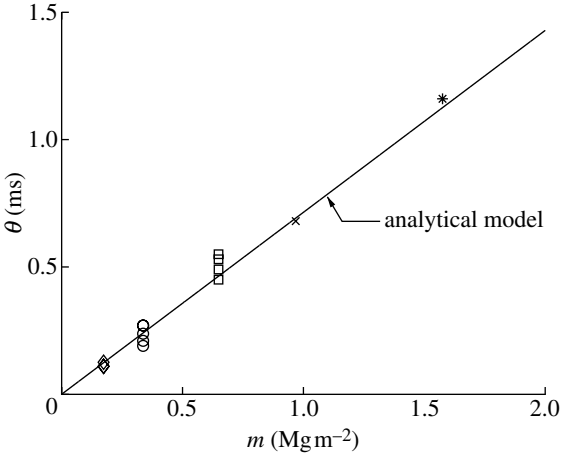

Figure 7. Comparison between the measured and predicted decay times θ as a function of the combined piston and projectile mass per unit area m. The multiple data points at each m value correspond to tests with different velocities v_o, see figure 6.

included in figure 7. The measurements support the prediction and indicate that θ increases linearly with m and is approximately independent of the striker velocity.

4. One-dimensional fluid–structure interaction of sandwich panels

Taylor (1941) computed the momentum transmitted to a free-standing plate by the impingement of a one-dimensional shock wave. Fleck & Deshpande (2004) followed this approach and computed the momentum transmitted to a sandwich plate by treating the front face of the sandwich plate as a free-standing plate

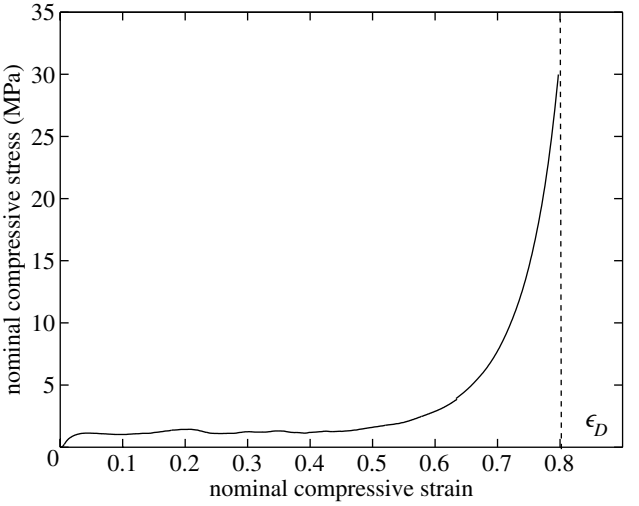

Figure 8. The quasi-static compressive stress versus strain response of the Alporas metal foam.

without support of the core during this FSI phase. Refinements by Deshpande & Fleck (2005) and Hutchinson & Xue (2005) suggest that a larger fraction of the underwater shock momentum is transmitted into the sandwich than suggested by the Taylor (1941) analysis for a free-standing front face sheet. Here, we employ the underwater shock simulator described above to measure the level of FSI for sandwich plates with steel faces and an aluminium alloy foam core.

(*a*) *Experimental investigation*

Circular sandwich plates comprising Alporas[2] aluminium alloy foam cores and mild steel face sheets were employed. The sandwich plates of diameter $D=45$ mm comprised two identical mild steel face sheets of density $\rho_f=8000$ kg m^{-3}. The Alporas aluminium foam core has a density $\rho_c=236$ kg m^{-3} and a thickness $c=25$ mm. Two sandwich configurations were employed, one with face sheets of thickness $h=6$ mm and one with $h=12$ mm. The front face sheet of the sandwich plate that faces the incoming underwater shock pulse provided sealing of the water column. To facilitate this, the face sheet was machined with a circumferential square groove of dimension 3×3 mm and fitted with an O-ring seal (figure 2*b*).

(i) *Material properties*

The quasi-static nominal compressive stress versus nominal compressive strain response of the Alporas foam is plotted in figure 8 for an applied strain-rate of 10^{-3} s^{-1}. This quasi-static response was measured using a cylindrical specimen similar to that used in the sandwich plates (diameter 45 mm and height 25 mm). The foam has a plateau stress of approximately 1.5 MPa and begins to densify at a nominal compressive strain $\epsilon\approx0.6$. The densification strain of $\epsilon_D=0.8$ is defined

[2] Shinko Wire Co. Ltd, Amagasaki, Japan.

(arbitrarily) by the strain at which the foam strength is 10 times the plateau strength.

Numerous experimental studies have shown that the Alporas metal foam has a negligible strain-rate sensitivity (Dannemann & Lankford 2000; Miyoshi *et al.* 2002), and that shock wave propagation in these foams becomes very important for impact velocities exceeding about 50 m s^{-1} (Radford *et al.* 2005). Details on the algorithm employed in the FE simulations to capture the strain rate and shock wave effects are given in §4*b*(i).

(ii) *Specimen manufacture and measurement protocol*

The sandwich plates were manufactured as follows. Circular cylinders of the Alporas foam, of diameter 45 mm and height 25 mm, were electro-discharged machined from blocks of foam. Mild steel face sheets were degreased and abraded, and were then adhered to the foam core using Redux 322 epoxy adhesive on a nylon carrier mesh. Bonding was facilitated by heating the plates in air at 175 °C for 1.5 h, with dead-loading imposed to give a nominal contact pressure of 0.01 MPa. The O-ring was then fitted in the groove on the front face sheet and the sandwich plate was inserted into the water tube. The sandwich plate was free to slide within the tube (the O-ring seal gave minimal resistance to sliding) and thus the experiment can be considered to be one-dimensional for all practical purposes. The rear face of the sandwich plate was located within the tube and positioned 20 mm from its end so that the FSI event has ended before the sandwich plate has popped out of the tube. After the insertion of the sandwich plate, the tube is filled with water and the loading piston is inserted at the opposite end, as described in §3. Pressure pulses with decay times $\theta = 0.12$ and 0.24 ms were generated in the water tube by firing steel projectiles of mass $m_1 = 0.236$ and 0.463 kg, respectively. These projectiles were fired with velocities v_p in the range 12–60 m s^{-1} to generate peak pressures p_o of 15–80 MPa.

Taylor (1941) showed that the level of FSI is set by the value of the following non-dimensional group:

$$\psi \equiv \frac{\rho_w c_w \theta}{\rho_f h}. \tag{4.1}$$

Thus, the experiments performed on the $h = 6$ mm sandwich plates had ψ-values of 3.5 and 7.0 while the tests on the $h = 12$ mm sandwich plates had ψ-values of 1.75 and 3.5.

(iii) *Experimental results*

After shock loading of each sandwich plate, the permanent reduction of core thickness Δc was measured, and the nominal core compression strain $\epsilon_c \equiv \Delta c / c$ was thereby measured. The measured core compression ϵ_c for the $h = 6$ mm sandwich plates is plotted in figure 9 as a function of the shock impulse $I_o = 2 p_o \theta$ for ψ equal to 3.5 and 7.0. The core compression increases with increasing I_o but full densification ($\epsilon_c = \epsilon_D$) is never achieved for the levels of shock impulses applied here. For a given I_o, the core compression is less for the $\psi = 7.0$ shock pulse than for the $\psi = 3.5$ shock pulse, as anticipated by the Taylor (1941) analysis.

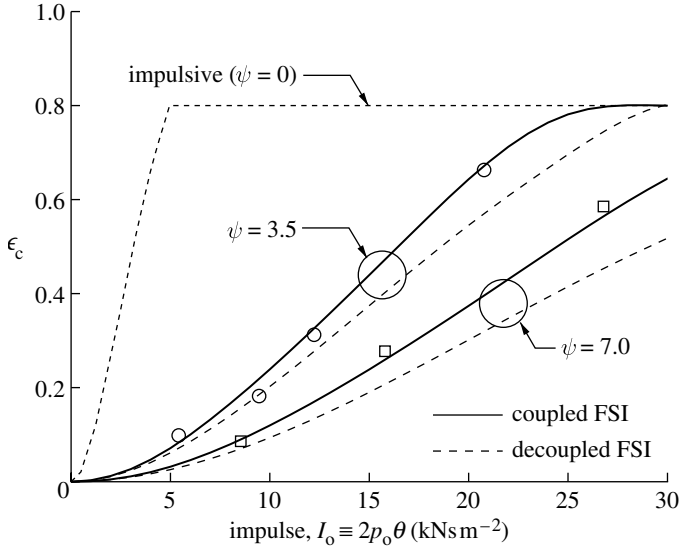

Figure 9. Comparison between the measured and predicted core compression for the unsupported metal foam sandwich with $h=6$ mm thick steel faces.

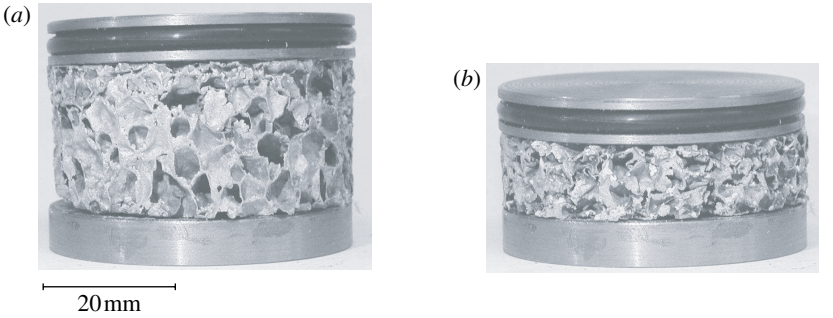

Figure 10. Photographs of the deformed foam core sandwich specimens with $h=6$ mm thick steel faces subjected to shock impulses with $\psi=7.0$ and (*a*) $I_o \approx 8$ kNs m^{-2} and (*b*) $I_o \approx 25$ kNs m^{-2}.

Photographs of the deformed sandwich plates subjected to shock impulses $I_o \approx 8.0$ and 25 kNs m^{-2} with $\psi=7.0$ are included in figure 10*a*,*b*, respectively. Figure 10*a* shows that the deformation of the foam core in these tests is non-uniform with the foam adjacent to the front face sheet fully compressed and the remainder of the foam undergoing negligible plastic deformation. This suggests that the core compresses by the passage of a plastic shock wave into the core from the front face sheet. The existence of a plastic shock wave is supported by the following observation. Recall that the foam core sandwich plates are loaded with peak pressures in the range 15–80 MPa. Quasi-static loading to such pressures would result in core compressions $\epsilon_c \approx 0.8$ (cf. figure 8) while much smaller core compressions are observed in the underwater shock experiments. The strength enhancement of the foam core due to the propagation of a shock wave explains this observation. The measured core compression ϵ_c for the

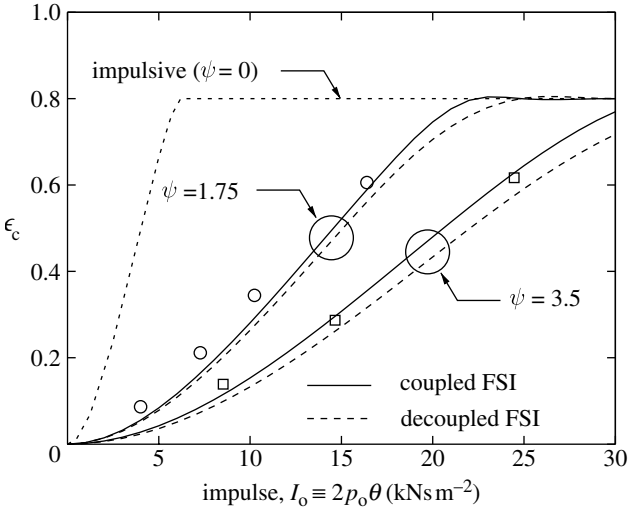

Figure 11. Comparison between the measured and predicted core compression for the unsupported metal foam sandwich with $h=12$ mm thick steel faces.

$h=12$ mm sandwich plates is plotted in figure 11 as a function of the shock impulse I_o for $\psi=1.75$ and 3.5. Again, ϵ_c increases with increasing I_o and decreases with increasing ψ.

(*b*) *Models for the fluid–structure interaction of sandwich plates*

Two models for the one-dimensional FSI of metal foam core sandwich plates are presented in this section. The first is a fully coupled model while the second model decouples the FSI phase from the core compression phase.

(i) *Coupled fluid–structure interaction model*

A FE scheme is now developed in order to model the full one-dimensional FSI problem, for an incoming shock wave in the fluid, and the ensuing wave propagation within the fluid and within each layer of the sandwich plate. The FE method is a convenient technique as it is able to handle:

(i) FSI after first cavitation,
(ii) multiple reflections of elastic waves within the faces and
(iii) the nonlinear dynamic response of the core.

An updated Lagrangian scheme is employed with the current configuration at time t serving as the reference. The coordinate x denotes the position of a material point in the current configuration with respect to a fixed Cartesian frame, and u is the displacement of that material point. For the one-dimensional problem under consideration, the principle of virtual work (neglecting effects of gravity) for a volume V and surface S is written in the form

$$\int_V \sigma\delta\epsilon \,\mathrm{d}V = \int_S T\delta u \,\mathrm{d}S - \int_V \rho \frac{\partial^2 u}{\partial t^2}\delta u \,\mathrm{d}V, \tag{4.2}$$

where σ is the Cauchy stress, $\epsilon \equiv \partial u/\partial x$ is the strain, T is the traction on the surface S of the current configuration and ρ is the material density in the current configuration.

A FE discretization based on linear, one-dimensional elements is employed. When the FE discretization of the displacement field is substituted into the principle of virtual work (4.2) and the integrations are carried out, the discretized equations of motion are obtained as

$$\boldsymbol{M}\frac{\partial^2 \boldsymbol{U}}{\partial t^2} = \boldsymbol{R}, \tag{4.3}$$

where $\boldsymbol{U}$ is the vector of nodal displacements, $\boldsymbol{M}$ is the mass matrix and $\boldsymbol{R}$ is the nodal force vector. A lumped mass matrix is used in (4.3) instead of a consistent mass matrix since this is preferable for explicit time integration procedures, for both accuracy and computational efficiency (Krieg & Key 1973). An explicit time integration scheme, based on the Newmark β-method with $\beta = 0$, is used to integrate equation (4.3) to obtain the nodal velocities and displacements, see Xu & Needleman (1994) for further details. Typically, there are 40 000 one-dimensional elements in the fluid, 2000 in the core and 200 in each face sheet.

The one-dimensional boundary value problem analysed is sketched in figure 12 and comprises a sandwich plate and a fluid column of height H_f. The sandwich plate comprises identical face sheets of thickness h and a core of thickness c. The face sheets of the sandwich plate are made from an elastic solid with Young's modulus $Ef = 210$ GPa and density $\rho_\mathrm{f} = 8000\ \mathrm{kg\ m^{-3}}$, which is representative of steel. The core is modelled as an elastic–plastic rate dependent solid of density $\rho_\mathrm{c} = 236\ \mathrm{kg\ m^{-3}}$. The total logarithmic strain rate in the core $\dot{\epsilon}$ is written as the sum of an elastic logarithmic strain rate $\dot{\epsilon}^\mathrm{e}$ and a plastic logarithmic strain rate $\dot{\epsilon}^\mathrm{p}$, so that at the stress level σ,

$$\dot{\epsilon} = \dot{\epsilon}^\mathrm{e} + \dot{\epsilon}^\mathrm{p}\ \mathrm{sign}(\sigma). \tag{4.4a}$$

The elastic strain rate is related to the stress rate by

$$\dot{\epsilon}^\mathrm{e} = \frac{\dot{\sigma}}{E_\mathrm{c}}, \tag{4.4b}$$

in terms of the Young's modulus $E_\mathrm{c} = 1$ GPa of the core. An overstress visco-plastic model is taken for the plastic strain rate,

$$\dot{\epsilon}^\mathrm{p} = \begin{cases} \left(\dfrac{|\sigma| - \sigma_c(\epsilon^p)}{\eta}\right), & \text{if } |\sigma| > \sigma_\mathrm{c}(\epsilon^\mathrm{p}) \text{ and } \epsilon^\mathrm{p} < \epsilon_\mathrm{D}, \\ 0, & \text{otherwise}, \end{cases} \tag{4.4c}$$

where $\sigma_\mathrm{c}(\epsilon^\mathrm{p})$ is the static yield strength at a plastic strain ϵ^p and η is the viscosity. The static yield strength σ_c versus plastic strain ϵ^p history is calibrated using the compressive stress versus strain response presented in figure 8 with complete lock-up of the foam assumed at $\epsilon^\mathrm{p} = \epsilon_\mathrm{D} = 0.8$. The value of viscosity η is set so that the shock width l_s is (Radford *et al.* 2005)

$$l_\mathrm{s} = \frac{\eta \epsilon_\mathrm{D}}{\rho \Delta v} = \frac{c}{10}, \tag{4.4d}$$

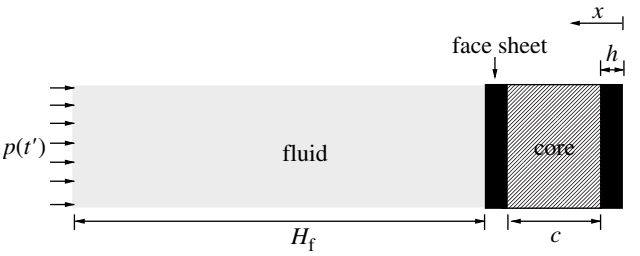

Figure 12. Boundary value problem analysed in the coupled one-dimensional finite element fluid–structure interaction simulations. In the supported case, a displacement $u=0$ is specified at $x=0$.

where Δv is the velocity jump across the shock. Here, we employ the estimate $\Delta v = p_o\theta/\rho_f h$ based upon a free-standing front face sheet. Large gradients in stress and strain occur over the shock width and thus a mesh size $e \leq l/10$ is chosen in the foam core to resolve these gradients accurately.

Following Bleich & Sandler (1970), the fluid medium in this one-dimensional analysis is modelled as a bilinear elastic solid with density $\rho_w = 1000\ \mathrm{kg\ m^{-3}}$ and modulus $E_w = 1.96$ GPa giving a wave speed $c_w \equiv \sqrt{E_w/\rho_w} = 1400\ \mathrm{m\ s^{-1}}$, which is representative of water. In particular, the stress σ versus logarithmic strain ϵ relationship is taken to be

$$\sigma = \begin{cases} E_w\epsilon, & \epsilon \leq 0, \\ 0, & \epsilon > 0, \end{cases} \tag{4.5}$$

so that the fluid is incapable of sustaining tensile stress. The sandwich plate dimensions are chosen to match the experiments, that is $c = 25$ mm and $h = 6$ or 12 mm.

A pressure history,

$$p = p_o e^{-t'/\theta}, \tag{4.6}$$

is applied to the top of the fluid column as shown in figure 12. Here, the time t' is measured from the instant of application of the pressure to the top of the fluid column. In contrast, the time t is measured from the instant that the shock wave impinges on the structure. The two are related by $t' = t + (H_f/C_w)$. In all calculations reported here, the height H_f of the water column is taken to be sufficiently large that the reflected wave does not reach the top of the water column over the duration of the calculations reported. Thus, the column can be considered to be semi-infinite. FE calculations with peak pressures ranging from $p_o = 2$ to 200 MPa and two values of the pulse decay constant $\theta = 0.12$ and 0.24 ms are reported below.

The FE predictions of the time evolution of the nominal through-thickness core strain for the $h = 6$ mm sandwich plate subjected to a shock pulse with $\theta = 0.24$ ms are plotted in figure 13 for three selected values of the peak pressure p_o. These curves indicate that only small elastic vibrations occur after the peak strain has been attained. We define ϵ_c as the peak value of nominal core strain over the time history.

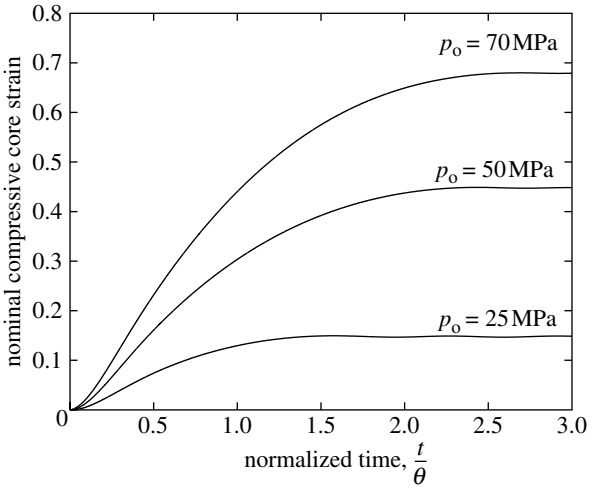

Figure 13. Finite element predictions of the time evolution of the nominal through-thickness core compression of the $h=6$ mm unsupported sandwich plate subjected to a shock pulse with $\theta=0.24$ ms ($\psi=7.0$).

The FE predictions of the permanent core compression ϵ_c for the $h=6$ and 12 mm sandwich plates are included in figures 9 and 11, respectively (solid lines mark coupled FSI). It is seen that the FE predictions are in excellent agreement with the measurements.

(ii) *Decoupled fluid–structure interaction model*

The decoupled model assumes that the response of the sandwich plate can be split into two sequential stages: stage I is the FSI problem during the blast event, and results in a uniform velocity being imposed on the front face sheet while stage II is the phase of core crush, during which the velocities of the faces and core equalize by momentum transfer.

Stage I: FSI phase. Taylor (1941) developed the solution for a one-dimensional underwater wave impinging a free-standing plate to compute the momentum transmitted to the plate by the shock pulse. Fleck & Deshpande (2004) followed this approach and similarly computed the momentum transmitted to a sandwich plate by treating the front face of the sandwich plate as a free-standing plate decoupled from the core and the rear face sheet. Here, we briefly review the relevant equations.

When the pressure wave (2.1) hits a stationary rigid plate at normal incidence it imparts an impulse I_o,

$$I_o = 2\int_0^\infty p_o e^{-t/\theta}\,\mathrm{d}t = 2p_o\theta, \tag{4.7}$$

to the plate. The factor of two arises in relation (4.7) due to full reflection of the pressure wave. If, instead, the pressure wave impacts a free-standing plate, the imparted impulse is less than I_o, and can be estimated as follows. When the pressure wave strikes a free-standing plate of thickness h made from a material of density ρ_f, it sets the plate in motion and is partly reflected. The reflected

wave becomes tensile with increasing plate velocity and when the net pressure at the interface between the plate and the fluid drops to zero cavitation sets in. The momentum per unit area I_{trans} transmitted into the structure is then given by

$$I_{\text{trans}} = \zeta I_{\text{o}}, \tag{4.8a}$$

where

$$\zeta \equiv \psi^{\psi/(1-\psi)}, \tag{4.8b}$$

and $\psi \equiv \rho_{\text{w}} C_{\text{w}} \theta / (\rho_{\text{f}} h)$. This impulse imparts a uniform velocity $v_{\text{o}} = I_{\text{trans}}/(\rho_{\text{f}} h)$ to the front face of the sandwich plate, with the core and rear face of the sandwich plate remaining stationary during this initial stage.

Stage II: core compression phase. In this phase, the presence of the fluid is neglected and the core is crushed by the advancing front face sheet. Consequently, the front face sheet is decelerated by the core while the core and the rear face of the sandwich beam are accelerated. We estimate the degree of core compression by performing FE calculations with an assumed velocity of the front face. The one-dimensional FE calculations are performed using the scheme described in §4*b*i with the sandwich plate material properties and dimensions identical to those employed in the coupled analysis. In these decoupled FE calculations, the fluid column is ignored and the loading is specified by imparting an initial uniform velocity $v_{\text{o}} = I_{\text{trans}}/(\rho_{\text{f}} h)$ to the front face sheet of the sandwich plate. The FE analysis gives the time evolution of the nominal through thickness compressive core strain and similar to the coupled analysis, we define ϵ_{c} as the peak core strain accumulated over the time history.

Predictions. The predictions of the decoupled analysis for the core compression ϵ_{c} are included in figures 9 and 11 (dashed lines mark decoupled FSI) for the $h = 6$ and 12 mm sandwich plates, respectively. The decoupled model under-predicts the measured core compression in all cases. This is consistent with the findings of Deshpande & Fleck (2005) and Hutchinson & Xue (2005): the Taylor free-standing plate analysis underestimates the shock impulse transmitted into sandwich plates, and consequently underestimates the degree of core compression.

The significance of the FSI is demonstrated by including predictions with $\psi = 0$ in figures 9 and 11. These FE calculations were performed by imparting an initial velocity $v_{\text{o}} = I_{\text{o}}/(\rho_{\text{f}} h)$ to the front face sheet. The $\psi = 0$ calculations predict a significantly higher ϵ_{c} than that measured in the experiments. For example, the $\psi = 0$ calculations for the $h = 6$ mm sandwich plates predict full densification at $I_{\text{o}} = 5$ kNs m^{-2} while the measured ϵ_{c} at $I_{\text{o}} = 5$ kNs m^{-2} is approximately equal to 0.1 and 0.05 for $\psi = 3.5$ and 7.0, respectively. This is clear and dramatic evidence that only a small fraction of the shock impulse is transmitted into the structure due to the FSI effect.

(*c*) *Effect of boundary conditions*

Recently, Dharmasena *et al.* (in preparation) have modified the Paddlewheel test apparatus to perform underwater explosive loading experiments on sandwich plates placed on a rigid foundation. Thus, unlike the experiments and analyses

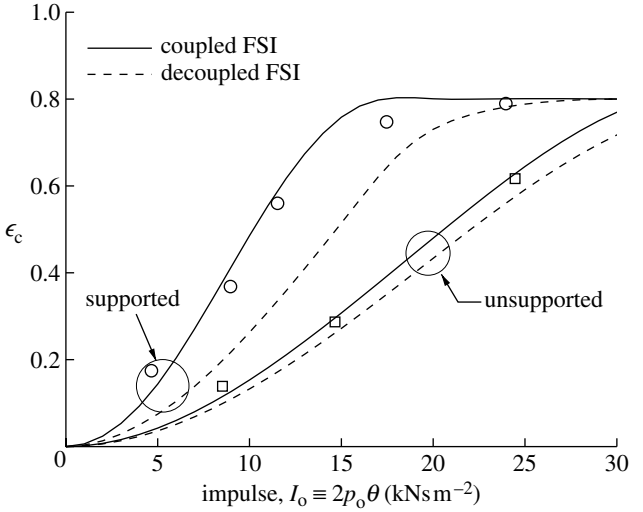

Figure 14. The effect of the boundary condition on the core compression of the $h=12$ mm sandwich with $\psi=3.5$. Predictions of the coupled and decoupled analyses are included.

reported above, the sandwich plates in those experiments were not free to translate. Here, we investigate the effect of this rigid foundation boundary condition upon the level of core compression of the $h=12$ mm sandwich plates subjected to shock pulses with $\theta=0.24$ ms ($\psi=3.5$).

The rigid foundation boundary condition was implemented experimentally as follows. The sandwich plate was inserted into the tube such that the rear face was flush with the tube end. The tube was then screw-capped by a 6 mm thick steel plate such that the rear face of the sandwich plate rested on this steel cap. The tube was then filled with water and the loading piston inserted as described in §3. We shall refer to this boundary condition in which sliding of the rear face of the sandwich plate was constrained as the 'supported' boundary condition while the experiments of §4*a* are labelled 'unsupported'. Pressure pulses with $\theta=0.24$ m and peak pressures p_o in the range 10–70 MPa were generated by firing a projectile of mass $m_1=0.463$ kg at velocities in the range 12–60 m s^{-1}.

The measured final core compression ϵ_c is plotted in figure 14 as a function of $I_o \equiv 2p_o\theta$ along with the corresponding measured values of ϵ_c for the experiments with the unsupported boundary condition (figure 11). Core compression is much larger with the supported boundary condition. For example, with the choice $I_o=15$ kNs m^{-2}, the core strain ϵ_c increases from 0.3 in the unsupported case to the densification value of 0.8 in the supported case.

Predictions of the core compression ϵ_c using the coupled and decoupled models are included in figure 14 for the supported case. The calculations were carried out in a manner similar to that described in §4*b* with a displacement $u=0$ specified on the node at $x=0$ (figure 12). The coupled calculations agree well with the measurements while the decoupled model under-predicts ϵ_c by as much as 75% in the supported case. Recall that with the unsupported boundary condition, the decoupled model under-predicts ϵ_c by only about 10%. This indicates that the continued loading of the sandwich plate after first cavitation is much more

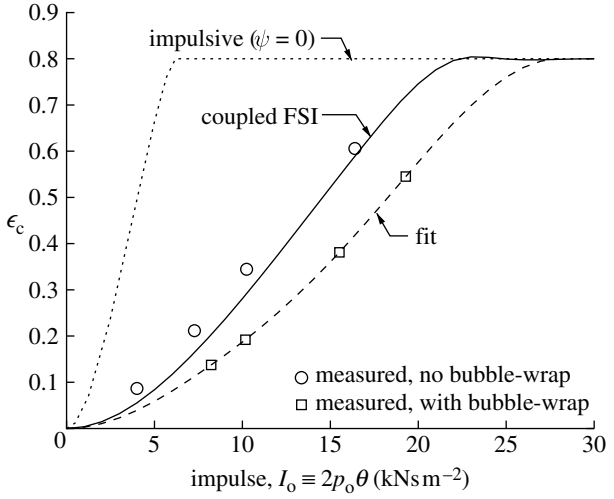

Figure 15. The effect on core compression of adding a layer of bubble-wrap on the wet surface of the front face sheet of the $h=12$ mm sandwich with $\psi=1.75$. The experiments were performed with the unsupported boundary condition.

important in the supported case compared to the unsupported case. An overlap of time scales occurs between the impingement of the shock wave on the front face and the period of core compression, and so a coupled analysis is required in the supported case.

5. Discussion

The experiments and calculations discussed above clearly demonstrate a strong FSI effect in the loading of sandwich plates by an underwater shock pulse. The shock impulse transmitted into the sandwich plate (and consequently the core compression) decreases with increasing value of the Taylor FSI parameter ψ. This suggests that reducing the acoustic impedance of the front face sheet could substantially reduce the momentum transmitted into the sandwich plate. While reducing the mass of the front face sheet would achieve this objective, in most cases this is not practical as a minimum face sheet thickness is required to withstand service loadings such as wave loading and occasional mild collisions. Strategies such as cladding the front face sheet with a soft layer (whose acoustic impedance is much less than that of water) might be a practical alternative. As an example, we demonstrate the effect of gluing a layer of bubble wrap on the front face of the sandwich plate.

The unsupported experiments on the $h=12$ mm sandwich plate with $\psi=1.75$ ($\theta=0.12$ ms) were repeated with a layer of bubble wrap glued on the wet surface of the front face sheet. The bubble wrap comprised a single layer of 8 mm diameter bubbles in a hexagonal close-packed arrangement. A comparison between the measured permanent core compression ϵ_c, with and without the layer of bubble wrap is shown in figure 15. At $I_o=15$ kNs m^{-2} there is nearly a 50% reduction in ϵ_c when a layer of bubble wrap is glued on the front face. This clearly demonstrates the beneficial effects of adding a low acoustic impedance

coating on the wet surface of the front face sheet. The development of strategies to enhance the FSI effect are suggested as a topic for future study.

6. Concluding remarks

A laboratory apparatus has been developed to simulate underwater shock loading. It comprises a water tube with a piston at one end and a test structure at the opposite end. Impact of the piston by a steel projectile generates an exponentially decaying shock pulse in the water; the peak pressure and pulse decay times are controlled independently by adjusting the striker velocity and mass, respectively. Analytical formulae are presented for the pressure versus time history generated in the water as a function of the striker velocity and mass. Good agreement between the predictions and measurements is observed.

The water tube has been employed to investigate the FSI of sandwich plates with steel face sheets and aluminium foam cores. A strong FSI effect is shown to exist, and a coupled FE analysis is able to capture the measured degree of core compression. In contrast, a decoupled model based upon the Taylor free-standing plate analysis underestimates the degree of core compression. The beneficial effects of adding a soft cladding on the front face sheet are demonstrated: a layer of bubble wrap on the wet surface of the front face sheet reduces the degree of core compression by up to 50%. Schemes to enhance the FSI effect are suggested as a topic for future study.

The authors are grateful to ONR for their financial support through US-ONR IFO grant number N00014-03-1-0283 on The Science and Design of Blast Resistant Sandwich Structures.

References

Bleich, H. H. & Sandler, I. S. 1970 Interaction between structures and bilinear fluids. *Int. J. Solids Struct.* **6**, 617–639. (doi:10.1016/0020-7683(70)90034-X)

Dannemann, K. A. & Lankford, J. 2000 High strain rate compression of closed-cell aluminium foams. *Mater. Sci. Eng. A* **293**, 157–164. (doi:10.1016/S0921-5093(00)01219-3)

Deshpande, V. S. & Fleck, N. A. 2005 One-dimensional shock response of sandwich beams. *J. Mech. Phys. Solids.* **53**, 2347.

Dharmasena, K. P., Queheillalt, D. T., Wadley, H. N. G., Dudt, P., Chen, Y. & Knight, D. In preparation. Dynamic compressive response under blast loading in water of periodic cellular structures.

Fleck, N. A. & Deshpande, V. S. 2004 The resistance of clamped sandwich beams to shock loading. *J. Appl. Mech.* **71**, 386. (doi:10.1115/1.1629109)

Florence, A. L. 1966 Circular plate under a uniformly distributed impulse. *Int. J. Solids Struct.* **2**, 37–47. (doi:10.1016/0020-7683(66)90005-9)

Gerard, G. 1956 A new experimental technique for applying impulsive loads, *Proc. Symp. on Impact Testing*, number 176 in *ASTM Special Technical Publication*, Atlantic City, NY, pp. 94–109.

Hutchinson, J. W. & Xue, Z. 2005 Metal sandwich plate optimized for pressure impulses. *Int. J. Mech. Sci.* **47**, 545–569. (doi:10.1016/j.ijmecsci.2004.10.012)

Krieg, R. O. & Key, S. W. 1973 Transient shell response by numerical time integration. *Int. J. Numer. Meth. Eng.* **7**, 273–286. (doi:10.1002/nme.1620070305)

Menkes, S. B. & Opat, H. J. 1973 Broken beams. *Exp. Mech.* **13**, 480–486.

Miyoshi, T., Mukai, T. & Higashi, K. 2002 Energy absorption in closed-cell Al–Zn–Mg–Ca–Ti foam. *Mater. Trans.* **43**, 1778–1781. (doi:10.2320/matertrans.43.1778)

Nurick, G. N. & Martin, J. B. 1989*a* Deformation of thin plates subjected to impulsive loading—a review. Part 2: experimental studies. *Int. J. Impact Eng.* **8**, 170–186.

Nurick, G. N. & Martin, J. B. 1989*b* Deformation of thin plates subjected to impulsive loading—a review. Part 2: theoretical considerations. *Int. J. Impact Eng.* **8**, 159–170. (doi:10.1016/0734-743X(89)90014-6)

Olsona, M. D., Nurick, G. N. & Fagnana, J. R. 1993 Deformation and rupture of blast loaded square plates: predictions and experiments. *Int. J. Impact Eng.* **13**, 279–291. (doi:10.1016/0734-743X(93)90097-Q)

Rabczuk, T., Kim, J. Y., Samaniego, E. & Belytschko, T. 2004 Homogenization of sandwich structures. *Int. J. Numer. Meth. Eng.* **61**, 1009–1027. (doi:10.1002/nme.1100)

Radford, D. D., Deshpande, V. S. & Fleck, N. A. 2005 The use of metal foam projectiles to simulate shock loading on a structure. *Int. J. Impact Eng.* **31**, 1152–1171. (doi:10.1016/j.ijimpeng.2004.07.012)

Ramajeyathilagam, K. & Vendhan, C. P. 2004 Deformation and rupture of thin rectangular plates subjected to underwater shock. *Int. J. Impact Eng.* **30**, 699–719. (doi:10.1016/j.ijimpeng.2003.01.001)

Ramajeyathilagam, K., Vendhan, C. P. & Rao, V. B. 2000 Non-linear transient dynamic response of rectangular plates under shock loading. *Int. J. Impact Eng.* **24**, 999–1015. (doi:10.1016/S0734-743X(00)00018-X)

Stoffel, M., Schmidt, R. & Weichert, D. 2001 Shock wave-loaded plates. *Int. J. Solids Struct.* **38**, 7659–7680. (doi:10.1016/S0020-7683(01)00038-5)

Swisdak, M. M. 1978 Explosion effects and properties: part II—explosion effects in water. Technical report, Naval surface weapons centre, Dahlgren, Virginia, USA.

Taylor, G. I. 1941 The pressure and impulse of submarine explosion waves on plates. In *The scientific papers of G I Taylor, vol. III*, pp. 287–303. Cambridge: Cambridge University Press, 1963.

Xu, X. P. & Needleman, A. 1994 Numerical simulations of dynamic crack-growth along an interface. *J. Mech. Phys. Solids* **42**, 1397–1434. (doi:10.1016/0022-5096(94)90003-5)

Xue, Z. & Hutchinson, J. W. 2004 A comparative study of blast-resistant metal sandwich plates. *Int. J. Impact Eng.* **30**, 1283–1305. (doi:10.1016/j.ijimpeng.2003.08.007)